

UNIVERSITY OF CALIFORNIA

Los Angeles

Experimental Characterization of High Impedance
Electromagnetic Surfaces in the Microwave Frequency Regime

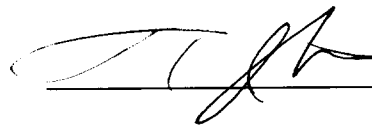
A thesis submitted in partial satisfaction
of the requirements for the degree Master of Science
in Electrical Engineering

by

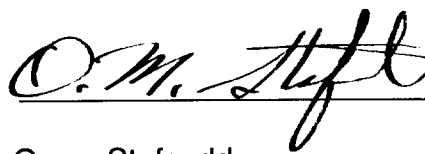
Romulo Francis Jimenez Broas

1999

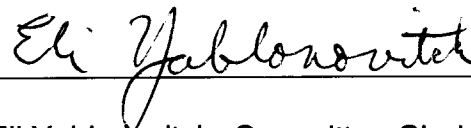
The thesis of Romulo Francis Jimenez Broas is approved.

A handwritten signature in black ink, appearing to be 'T. Itoh', written over a horizontal line.

Tatsuo Itoh

A handwritten signature in black ink, appearing to be 'O. M. Stafsudd', written over a horizontal line.

Oscar Stafsudd

A handwritten signature in black ink, appearing to be 'Eli Yablonovitch', written over a horizontal line.

Eli Yablonovitch, Committee Chair

University of California, Los Angeles

1999

To my parents,
Emelita and Levy,
whom I love, honor, and thank
from the bottom of my heart

Table of Contents

Chapter 1: Introduction	...page 1
Chapter 2: Design	...page 4
Chapter 3: Measurement of the Photonic Band-Gap Using TE Waves	...page 10
Chapter 4: The High Impedance Electromagnetic Surface as an Antenna Radiation Shield	...page 13
4.1. Introduction.....	page 13
4.2. Experimental Setup.....	page 14
4.3. Method of Analysis.....	page 17
4.4. Experimental Results and Analysis.....	page 22
Chapter 5: Application of High Impedance Electromagnetic Surfaces to Phased Arrays	...page 31
5.1. Introduction.....	page 31
5.2. Experimental Setup.....	page 32
5.3. Experimental Results and Analysis.....	page 35
5.4. Summary.....	page 43
Chapter 6: Conclusion	...page 45
References	...page 46

List of Figures

- Figure 1.1: The three-layer structure.....page 1
- Figure 1.2: Solenoidal properties of the high impedance electromagnetic surface.....page 2
- Figure 2.1: Three-layer hexagonal structure.....page 4
- Figure 2.2: Area of the parallel plates.....page 5
- Figure 2.3: Relevant dimensions of the three-layer hexagonal structure.....page 5
- Figure 3.1: Experimental setup to measure the transmission of TE surface wavespage 10
- Figure 3.2: Measurement of the transmission of TE surface waves for the three-layer hexagonal structure.....page 11
- Figure 4.1: Experimental setup to measure the antenna radiation of an antenna using a high impedance electromagnetic surface as a ground plane.....page 15
- Figure 4.2: A cordless telephone prototype using a high impedance electromagnetic surface as a ground plane.....page 16
- Figure 4.3: Measurement of the radiation transmission between the horn and antenna on a high impedance electromagnetic surface. The frequency is 2.44 GHz.....page 19
- Figure 4.4: Measurement of the radiation transmission between two identical horns. The frequency is 2.44 GHz.....page 20
- Figure 4.5: Plot of FWHM versus frequency.....page 24

Figure 4.6: Plot of cross-section versus frequency.....page 25

Figure 4.7: Plot of front-to-back ratio versus frequency.....page 26

Figure 4.8: Plot of antenna efficiency versus frequency.....page 27

Figure 5.1: Experimental setup similar to the GPS configuration to study the suppression of surface waves by the high impedance electromagnetic surface.....page 33

Figure 5.2: Two antennas are in a straight line.....page 34

Figure 5.3: Two antennas are parallel to one another.....page 35

Figure 5.4: High impedance electromagnetic surface with antennas on a straight line. The frequencies plotted are inside the band-gap.....page 39

Figure 5.5: High impedance electromagnetic surface with antennas on a straight line. The frequencies plotted are outside the band-gap.....page 40

Figure 5.6: High impedance electromagnetic surface with antennas that are parallel to one another. The frequencies plotted are inside the band-gap.....page 41

Figure 5.7: High impedance electromagnetic surface with antennas that are parallel to one another. The frequencies plotted are outside the band-gap.....page 42

List of Table

Table 5.1: Summary of the standard deviations of the phase difference (in degrees) as a function of frequency (in GHz).....page 43

Acknowledgments

The author wishes to acknowledge the support and help of his advisor, Professor Eli Yablonovitch. With gratitude the author also wishes to acknowledge Dr. Daniel F. Sievenpiper, who carried out the pioneering work on high impedance electromagnetic surfaces along with Professor Eli Yablonovitch. Their vast accomplishments, scientific talents, prolific publications, and good natures have paved the way for this thesis.

A lot of the theory and ideas of this thesis are based on the doctoral dissertation of Dr. Sievenpiper. In particular, Figures 1.1, 1.2, 2.1, 2.3, and 3.1 are taken from his dissertation. The author would very much like to acknowledge this document by Dr. Sievenpiper.

Finally, the author gives the sincerest gratitude to his family, particularly his parents Levy M. Broas and Emelita J. Broas. His thanksgiving for his parents cannot be expressed in words.

ABSTRACT OF THE THESIS

Experimental Characterization of High Impedance Electromagnetic Surfaces in the Microwave Frequency Regime

by

Romulo Francis Jimenez Broas

Master of Science in Electrical Engineering

University of California, Los Angeles, 1999

Professor Eli Yablonovitch, Chair

A design procedure was performed in which a high impedance electromagnetic surface has a band-gap in the microwave frequency regime of 2.35 to 2.55 GHz. This band-gap was confirmed directly by experimental data.

The high impedance electromagnetic surface has the ability to suppress surface waves in the band-gap. If the high impedance electromagnetic surface is used as an antenna ground plane, then the propagation of radiation as surface waves will be minimized. Radiation will be confined to one hemisphere as the high impedance electromagnetic surface acts like a shield.

A cordless telephone prototype was built that employed a high impedance electromagnetic surface acting as the antenna ground plane. In the band-gap,

nearly all of the radiation is confined to one hemisphere. The peak gain of the antenna is higher and its radiation is more directional, and therefore the antenna efficiency is high. Outside the band-gap, a lot of the radiation leaks into the back of the antenna ground plane. The peak gain is lower, and the radiation not very directional. Hence, the antenna efficiency is low.

The suppression of surface waves by the high impedance electromagnetic surface can also be beneficial to phased arrays. If there are two or more antennas on the same high impedance electromagnetic surface, then the coupling between them will be reduced since surface wave propagation is major contributor to inter-element coupling. The phase difference due to inter-element coupling is substantially less inside the band-gap as opposed to outside the band-gap.

Chapter 1: Introduction

This thesis experimentally characterizes high impedance electromagnetic surfaces in the microwave frequency regime of 2.2 to 2.8 GHz. To have a photonic band-gap in this microwave frequency regime, a high capacitance is needed. This high capacitance is obtained by using two parallel metal plates with a thin insulating layer between them. Hence, a three-layer structure is employed in which the bottom metallic layer is a solid sheet and the two other metallic layers give the parallel plate capacitance. This is shown diagrammatically in the figure below, where the top two layers are effectively parallel plates that give a high parallel plate capacitance. The bottom layer is a solid metal sheet.

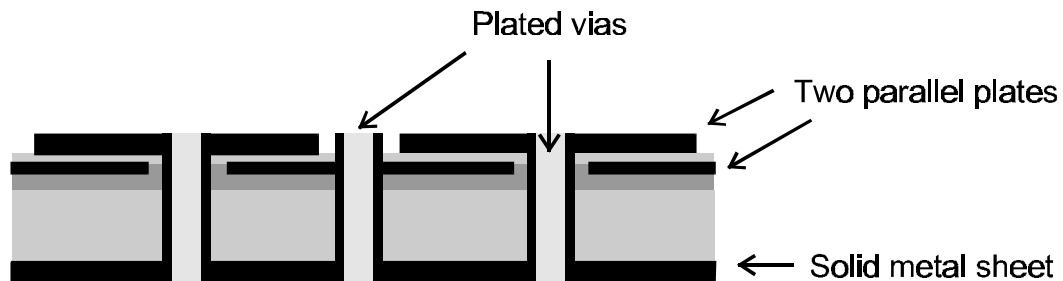


Figure 1.1: The three-layer structure (Reference 1).

Likewise, the high impedance electromagnetic surface exhibits properties of a solenoid with currents circulating around it as shown.

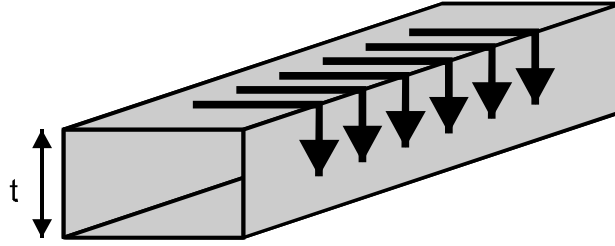


Figure 1.2: Solenoidal properties of the high impedance electromagnetic surface (Reference 1).

This solenoid has an inductance that is linearly dependent on the thickness t of the high impedance electromagnetic surface.

Because it has dual aspects of solenoids giving an inductance and parallel plates having a high capacitance, the high impedance electromagnetic surface can be modeled as an equivalent circuit. In particular, their properties are very much similar to parallel LC circuits having a resonant frequency equal to $\frac{1}{\sqrt{LC}}$, where L is the inductance given by its solenoidal properties and C is the parallel plate capacitance.

The resonant frequency of $\frac{1}{\sqrt{LC}}$ is the center of the photonic band-gap. In the photonic band-gap frequency range, the electromagnetic surface exhibits high surface impedance and does not conduct AC currents. As a result, the high impedance electromagnetic surface can be used as an antenna ground plane because it suppresses surface waves. In this thesis, two applications are discussed in which the suppression of surface waves is particularly beneficial:

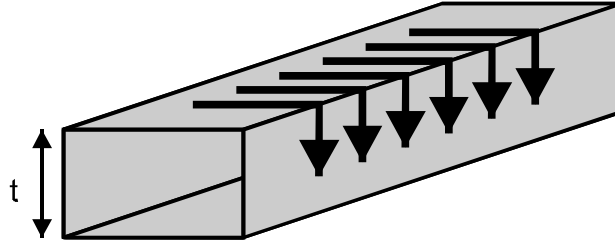


Figure 1.2: Solenoidal properties of the high impedance electromagnetic surface (Reference 1).

This solenoid has an inductance that is linearly dependent on the thickness t of the high impedance electromagnetic surface.

Because it has dual aspects of solenoids giving an inductance and parallel plates having a high capacitance, the high impedance electromagnetic surface can be modeled as an equivalent circuit. In particular, their properties are very much similar to parallel LC circuits having a resonant frequency equal to $\frac{1}{\sqrt{LC}}$, where L is the inductance given by its solenoidal properties and C is the parallel plate capacitance.

The resonant frequency of $\frac{1}{\sqrt{LC}}$ is the center of the photonic band-gap. In the photonic band-gap frequency range, the electromagnetic surface exhibits high surface impedance and does not conduct AC currents. As a result, the high impedance electromagnetic surface can be used as an antenna ground plane because it suppresses surface waves. In this thesis, two applications are discussed in which the suppression of surface waves is particularly beneficial:

- 1) **Cordless telephones:** the suppression of surface waves can effectively confine antenna radiation in only one hemisphere. This makes the high impedance electromagnetic surface act like a shield for a radiating antenna element.
- 2) **Phased arrays (as in the Global Positioning System architecture):** the suppression of surface waves reduces the detrimental coupling between neighboring antennas in phased arrays.

Experimental data from these two applications will be presented to prove the benefits of using the high impedance electromagnetic surface.

Chapter 2: Design

The high-impedance electromagnetic surface analyzed was the three-layer hexagonal structure shown below.

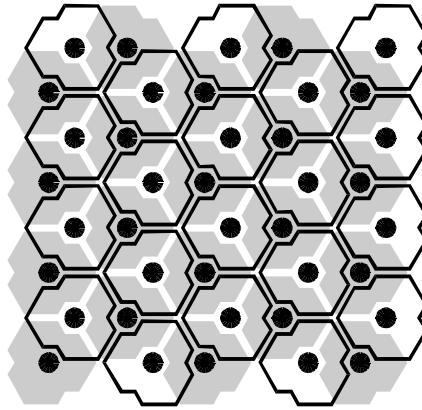


Figure 2.1: Three-layer hexagonal structure (Reference 1).

As described in the Introduction, these high impedance electromagnetic surfaces can be modeled as an equivalent circuit where there is capacitance and inductance. The capacitance is mainly given by parallel plates, where the area of the parallel plates to be considered is shown below.

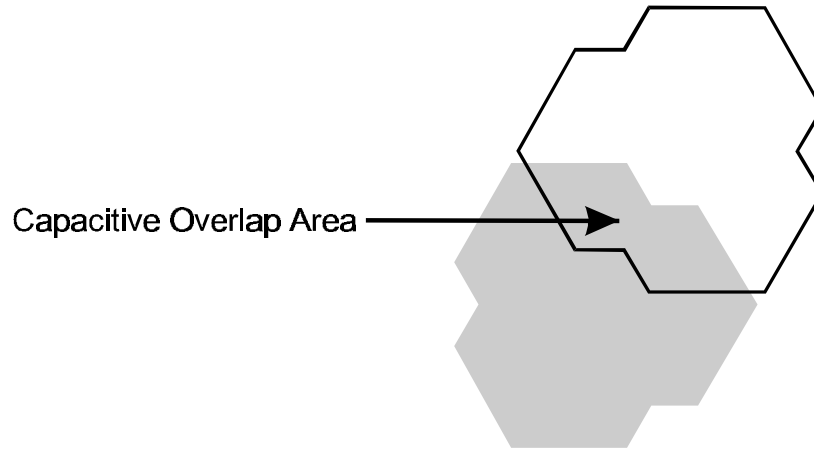


Figure 2.2: Area of the parallel plates.

This overlap area of the parallel plates can be obtained from the dimensions of the three-layer hexagonal structure. In particular, two parameters are of interest to obtain the capacitive overlap area: the distance between neighboring vias (a), and the overlap distance (a'). These two parameters are shown below.

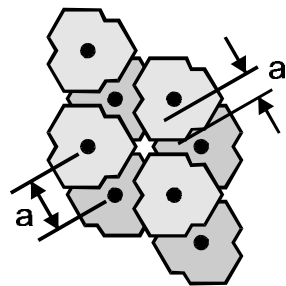


Figure 2.3: Relevant dimensions of the three-layer hexagonal structure (Reference 1).

For a distance between neighboring vias of 0.14434 inches and an overlap distance 0.085 inches, the capacitive overlap area is 0.0101 square inches, or 6.5161E-6 square meters. Between the parallel plates there is a layer of Kapton with a relative dielectric constant of 3.25 and a thickness of 2 mils inches (5.08E-5 meters). Hence, the individual parallel plate capacitance is readily calculated as follows:

$$\text{Capacitance} = C_i = \frac{\epsilon A}{d} = (3.25)(8.854\text{E-}12)(6.5161\text{E-}6)/(5.08\text{E-}5)$$

$$\text{Capacitance} = C_i = 3.6910\text{E-}12 \text{ Farads} = 3.6910 \text{ picroFarads}$$

Equation 2.1

The relevant capacitance for the equivalent LC circuit is the sheet capacitance resulting from the cumulative effect of the many individual parallel plate capacitances. The sheet capacitance C_s is easily calculated once the individual parallel plate capacitance C_i is known.

$$\text{Sheet Capacitance} = C_s = FC_i = F \frac{\epsilon A}{d} = \frac{1}{\sqrt{3}} \frac{\epsilon A}{d} = 2.1310 \text{ picroFarads}$$

Equation 2.2

In the calculation above, the geometrical factor F is equal to $\frac{1}{\sqrt{3}}$. The correction factor F is equal to $\frac{1}{\sqrt{3}}$ for all hexagonal geometries. The use of the geometrical factor is obligatory because capacitors oriented in different geometrical directions have different resonance frequencies even though they have the same capacitive value $C_i = \frac{\epsilon A}{d}$.

The sheet inductance given by the solenoidal properties of the high impedance electromagnetic surface is determined by the thickness of the board and the magnetic permeability. Since the thickness is 62 mils inches (0.0016 meters) and the permeability is of the order unity, the sheet inductance is calculated as follows:

$$L_s = \mu t = \mu_0 t = (4\pi \times 10^{-7})(0.0016) = 1.9790 \times 10^{-9} \text{ Henry} = 1.9790 \text{ nanoHenry}$$

Equation 2.3

With the inductance being 1.979 nH and the capacitance equal to 2.131 pF, the equivalent LC circuit has a resonant frequency equal to $\omega_b = \frac{1}{\sqrt{LC}}$. This resonant frequency also corresponds to the center of the photonic band-gap. The photonic band-gap bandwidth $\Delta\omega$ is readily obtained by the following equation:

$$\frac{\Delta\omega}{\omega_0} = \frac{\sqrt{\frac{L}{C}}}{\sqrt{\frac{\mu_0}{\epsilon_0}}}$$

Equation 2.4

Using $C = 2.1310$ pF, $L = 1.9790$ nH, and $\sqrt{\frac{\mu_0}{\epsilon_0}} = 376.7343$ H^{1/2}F^{-1/2}, the following calculations can be performed:

$$\omega_0 = \frac{1}{\sqrt{LC}} = 1.5399\text{E}10 \text{ Hz}$$

Equation 2.5

$$\Delta\omega = \omega_0 \frac{\sqrt{\frac{L}{C}}}{\sqrt{\frac{\mu_0}{\epsilon_0}}} = 1.2456\text{E}9 \text{ Hz}$$

Equation 2.6

Converting to ν via the equation $\nu = \omega/(2\pi)$, the upper and lower limits of the photonic band-gap is the following:

$$\nu_{\text{low}} = \frac{1}{2\pi} \left(\omega_0 - \frac{\Delta\omega}{2} \right) = 2.3517 \text{ GHz}$$

Equation 2.7

$$\nu_{\text{high}} = \frac{1}{2\pi} \left(\omega_0 + \frac{\Delta\omega}{2} \right) = 2.5499 \text{ GHz}$$

Equation 2.8

The center of the photonic band-gap is the following:

$$\nu_0 = \frac{\omega_0}{2\pi} = 2.4508 \text{ GHz}$$

Equation 2.9

In summary, the three-layer hexagonal structure shown in Figure 2.1 has physical dimensions that give a photonic band-gap from 2.3517 GHz to 2.5499 GHz.

Chapter 3: Measurement of the Photonic Band-Gap Using TE Waves

The calculations done in Chapter 2 designed a high impedance electromagnetic surface with a photonic band-gap from 2.35 to 2.55 GHz. In this chapter, the measurement of the photonic band-gap was done using TE waves.

The experimental methodology developed by Dr. Daniel Frederic Sievenpiper was performed. It uses two identical probes: one of the probes sends surface waves through the high impedance electromagnetic surface, and another probe measures the transmitted surface waves. The surface waves are mostly composed of TE waves. Essentially, the transmission of surface waves through the high impedance electromagnetic surface was measured.

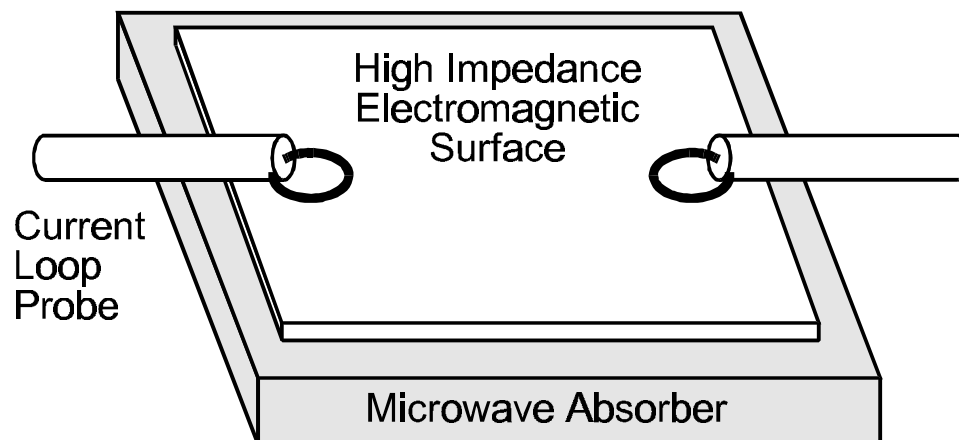


Figure 3.1: Experimental setup to measure the transmission of TE surface waves (Reference 1).

In the setup above, the transmission of TE surface waves can be experimentally determined. The band-gap, by definition, is the frequency regime where there is a suppression of surface waves. Hence, at the band-gap, the transmission of surface waves is minimized. Outside of the band-gap, the transmission of surface waves is substantially greater than in the band-gap.

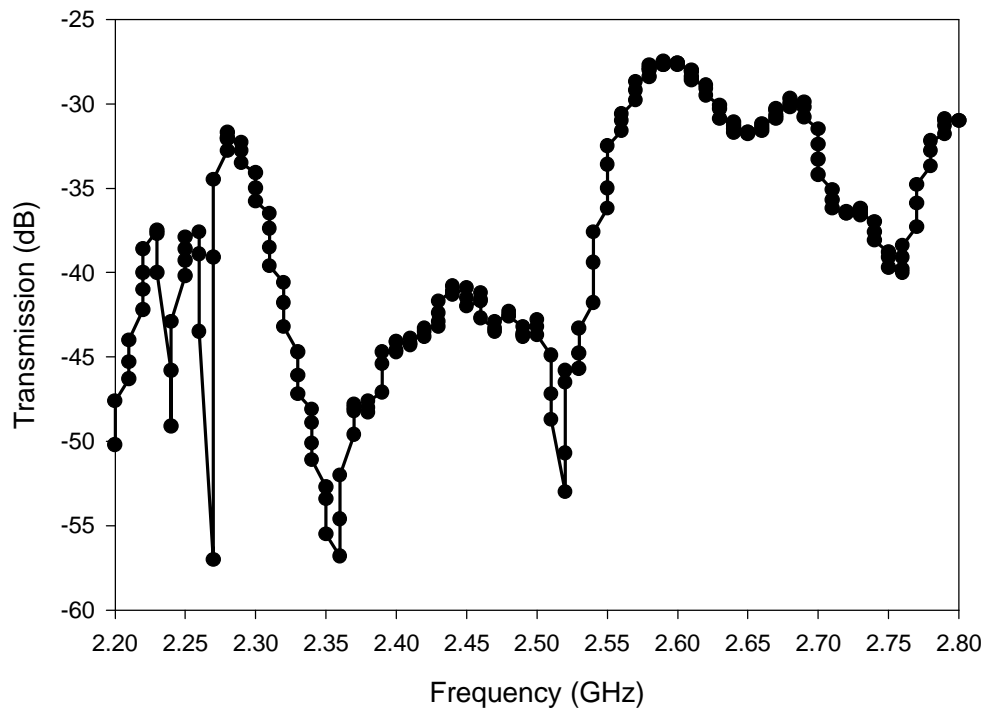


Figure 3.2: Measurement of the transmission of TE surface waves for the three-layer hexagonal structure.

In the setup above, the transmission of TE surface waves can be experimentally determined. The band-gap, by definition, is the frequency regime where there is a suppression of surface waves. Hence, at the band-gap, the transmission of surface waves is minimized. Outside of the band-gap, the transmission of surface waves is substantially greater than in the band-gap.

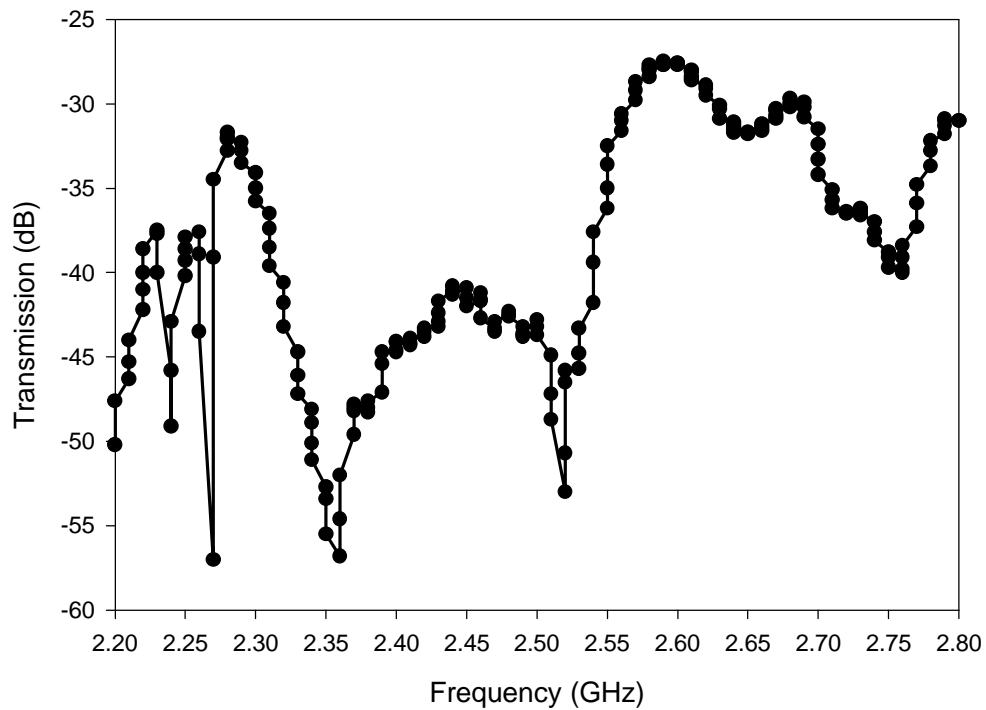


Figure 3.2: Measurement of the transmission of TE surface waves for the three-layer hexagonal structure.

The measurement of the transmission of TE surface waves for the three-layer hexagonal structure is shown in Figure 3.2. There is a lot of noise inherent in the experimental setup shown in Figure 3.1. Reflections and multi-path (the microwave regime's version of speckle in optical frequencies) are rampant. Nevertheless, the suppression of TE surface waves from 2.35 to 2.55 GHz cannot be denied. In this band-gap, the transmission of surface waves is more than 10 dBs less than the transmission outside the band-gap. There is a clear suppression of surface waves in the band-gap.

Chapter 4: The High Impedance Electromagnetic Surface as an Antenna Radiation Shield

4.1. Introduction

In Chapter 2, the design procedure for a three-layer hexagonal structure was examined. The particular dimensions of the structure gave it a photonic band-gap from 2.35 to 2.55 GHz. This band-gap was also measured in the experiment described in Chapter 3. In the band-gap frequency range, the equivalent LC circuit of the high impedance electromagnetic surface is in resonance so that there is a suppression of surface waves. If the high impedance electromagnetic surface is used as an antenna ground plane, then the propagation of antenna radiation as surface waves will be minimized. Therefore, antenna radiation will be confined to only one hemisphere as the high impedance electromagnetic surface acts like a shield that suppresses surface waves.

A promising application of using the high impedance electromagnetic surface as a radiation shield is in the cordless telephone industry. Current cordless telephone designs have nearly half of the emitted antenna radiation being absorbed by the user's head. While the biological implications of this are yet to be determined, it is well known that the absorption of the user's head decreases the antenna efficiency. This decrease poses strict requirements on the

battery of the cordless telephone by demanding more frequent battery charging and having batteries that are heavier in weight. However, if the high impedance electromagnetic surface is used as the antenna ground plane so that is the shield between the user's head and the radiating antenna, then the absorption will be greatly decreased. This will increase antenna efficiency, and power consumption will decrease.

4.2. Experimental Setup

The customary equipment and methods to measure antenna radiation were employed. The experimental setup is shown.

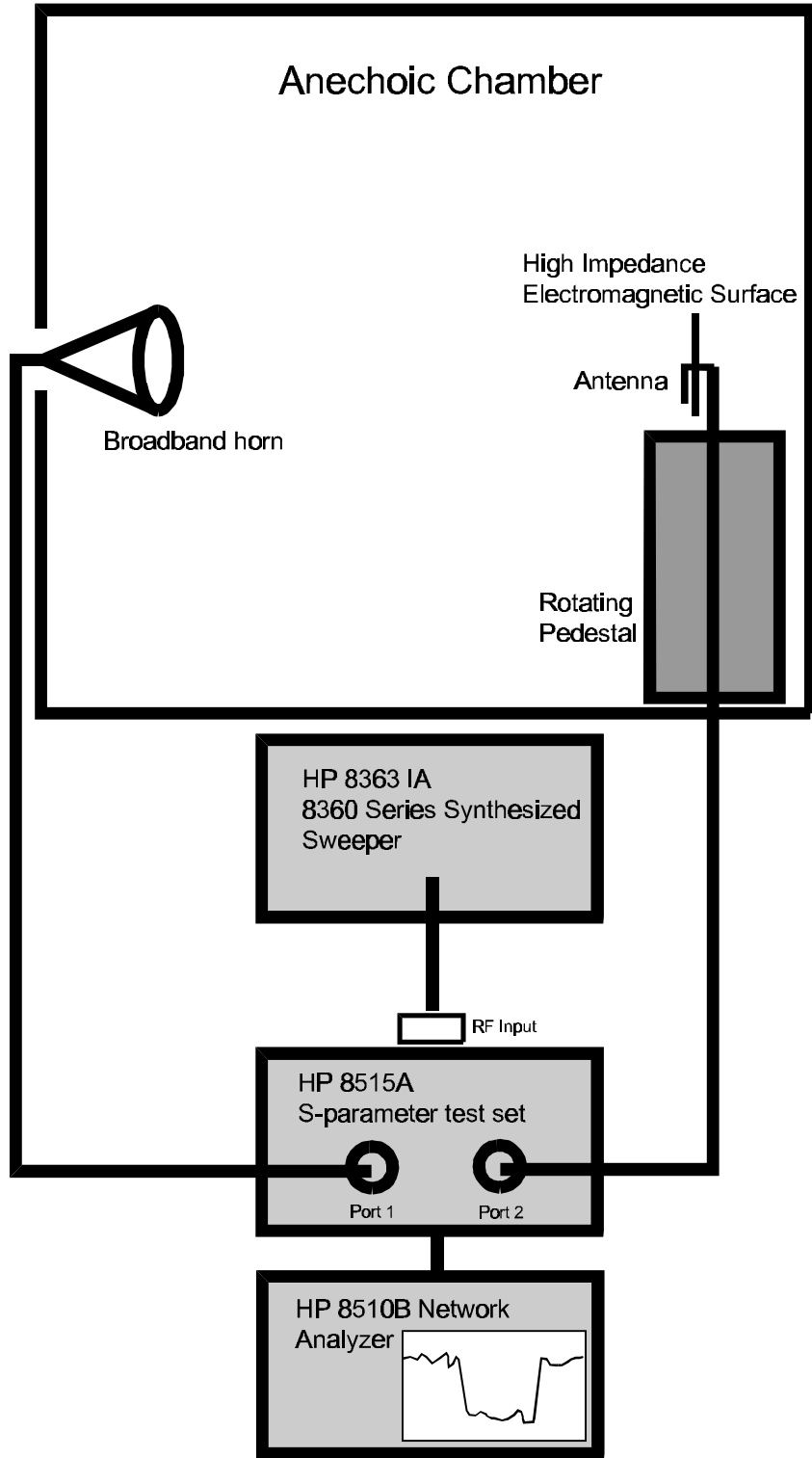


Figure 4.1: Experimental setup to measure the antenna radiation of an antenna using a high impedance electromagnetic surface as a ground plane.

The HP 8363 provides the RF input to the HP 8515, the S-parameter test set. The HP 8515, in turn, measures the S12 (or equivalently S21) parameter, which is the transmission between the horn and antenna. The transmission is measured in the anechoic chamber environment, where reflection is minimized. The data is displayed and acquired by the HP 8510, a network analyzer.

To simulate the cordless telephone, a prototype was built in which a FR4 circuit board (6 by 2 inches) was used, with one side having FR4 and the other side having copper. The copper side of the circuit board was then soldered to the solid metal sheet of the high impedance electromagnetic surface. The high impedance electromagnetic surface had dimensions of 1 by 2 inches, and with the antenna attached, it acted as the antenna ground plane.

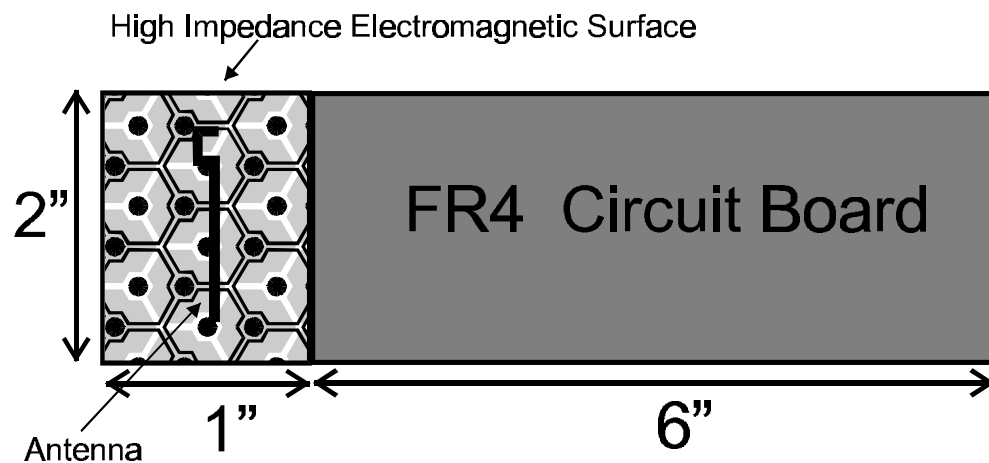


Figure 4.2: A cordless telephone prototype using a high impedance electromagnetic surface as a ground plane.

The prototype renders an accurate representation of the cordless telephone. The FR4 circuit board soldered to the high impedance electromagnetic surface simulates the complex electrical components that digitizes and processes the signals. The antenna functions in the wireless communication through space. The amount of space allotted to the high impedance electromagnetic surface, which is a mere 2 by 1 inches, is realistic as cordless telephones are being market-driven to be smaller and more lightweight.

The cordless telephone prototype shown in Figure 4.2 is mounted on the rotating pedestal as depicted in Figure 4.1. In this manner, a full angular view of the radiation is obtained as the prototype is rotated in a full circle. The full angular view allows the measurement of the antenna efficiencies, front-to-back ratios, full-width half-maximums, and cross-sections.

4.3. Method of Analysis

By measuring the radiation transmission between the horn and antenna as the pedestal rotated, the full angular view of the radiation was obtained. The data for such a measurement is shown in Figure 4.3 for the frequency 2.44 GHz. The angular scale is in degrees, and as can be seen, a full angular view of the

radiation was obtained as the rotation went from 0° to 360° . Measuring the radiation transmitted from the horn to the antenna, the radial scale is in dB's. The relative values of the radial scale are correct; for example, from one circle to the next nearest circle, the difference in the measured radiation is 10 dB. However, the absolute values of the transmission are obviously not correct. To get the absolute values, a comprehensive calibration is needed that encompasses the many variables in the experimental setup such as free space, cables, and gain of horn. An alternative method was used in which the efficiency is obtained in comparison to the horn efficiency. To do this, the full angular view of the horn radiation must also be done. Therefore, the measurement of the radiation transmitted between two identical horns was performed over the full angular view. The data for such a measurement is shown in Figure 4.4 for the frequency 2.44 GHz. Like Figure 4.3, the relative values of the transmission are correct but the absolute values are not.

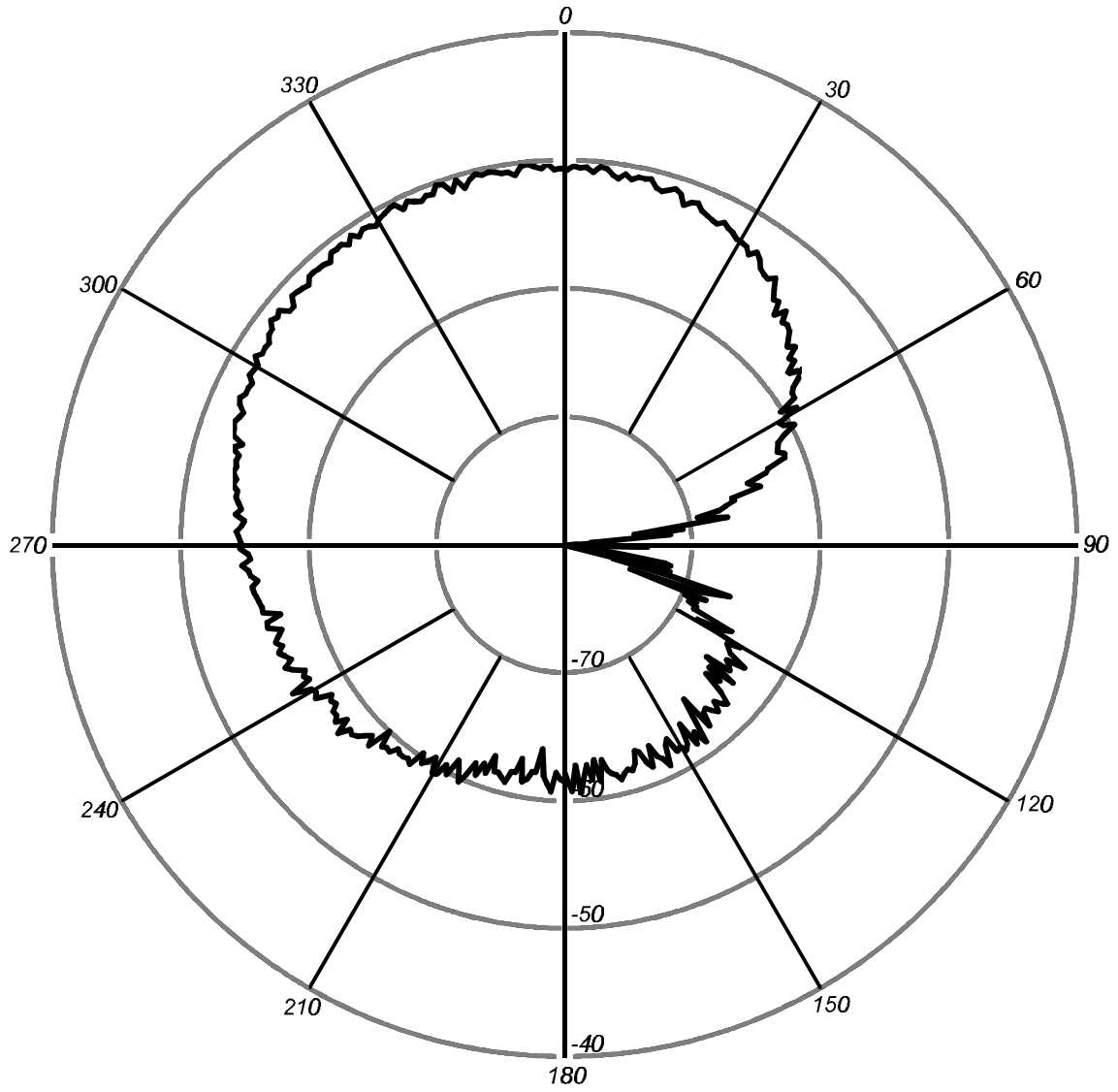


Figure 4.3: Measurement of the radiation transmission between the horn and antenna on a high impedance electromagnetic surface. The frequency is 2.44 GHz. At the zero degree polar angle, the cordless telephone prototype has its antenna facing the horn and its attached FR4 Circuit Board pointing towards the 270 degree polar angle. The cordless telephone prototype was subsequently

rotated in a full angular span to obtain the other polar angles while the receiving horn remained stationary.

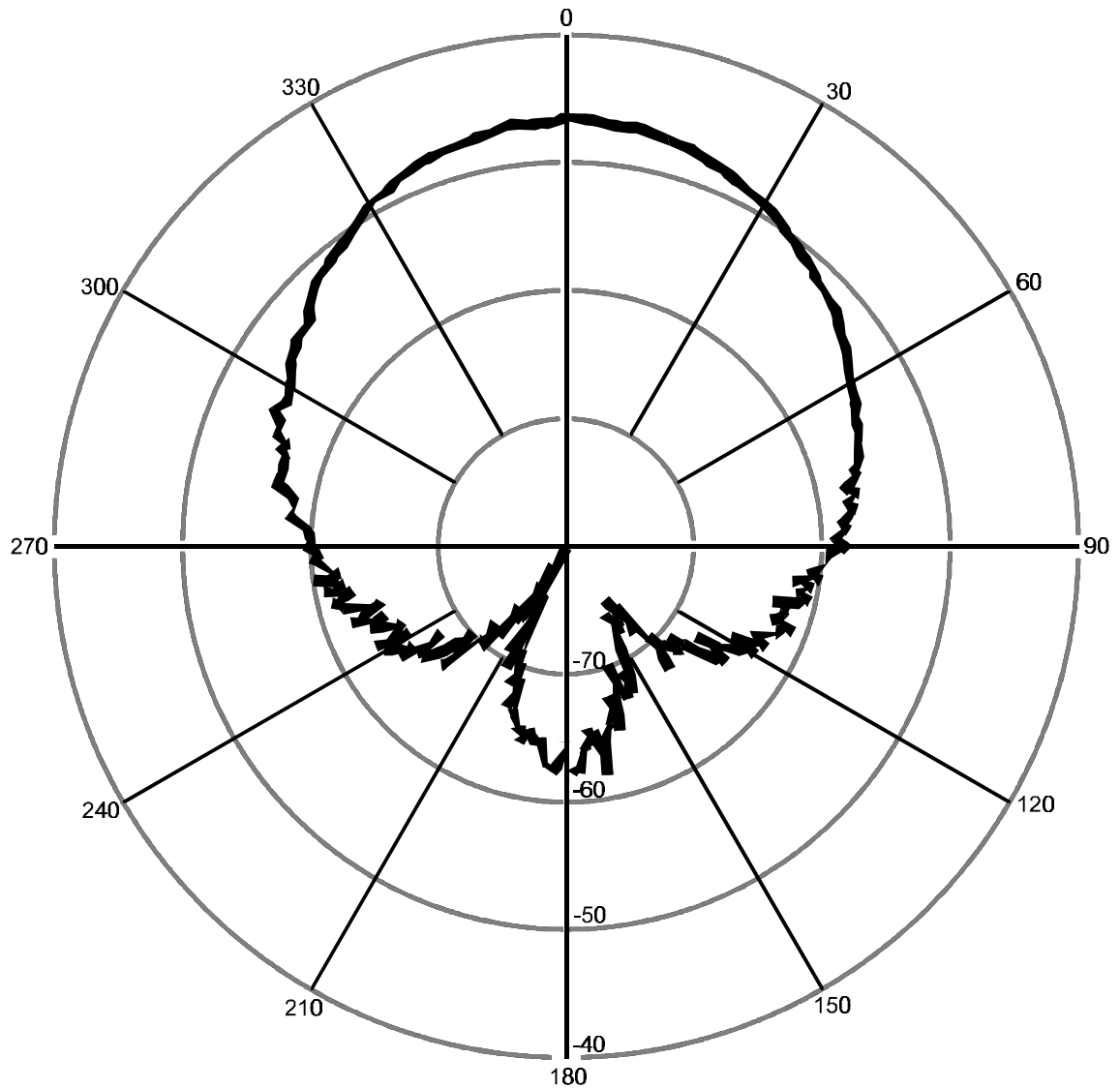


Figure 4.4: Measurement of the radiation transmission between two identical horns. The frequency is 2.44 GHz. At zero degree polar angle, the two horns are pointing towards one another.

With polar plots as shown in Figures 4.3 and 4.4, the full-width half-maximum (FWHM) values for various frequencies can be obtained. To do this is very simple: one first needs to find the peak transmission. Since 3 dB down is half the peak transmission, 3 dB is to be subtracted from the peak transmission. There are two angular values in the polar plot with a transmission value of 3 dB below the peak transmission. The angle between the points having a transmission value 3 dB below the peak transmission is the FWHM. By definition, FWHM has units of degrees.

Of particular interest is the cross-section associated with the FWHM. By definition (see Reference 2), the cross-section Ω is

$$\Omega = \int \frac{1}{r^2} dA = \int \frac{1}{r^2} (2\pi r \sin \theta)(r d\theta) = 2\pi \int_{\theta=0}^{\theta=FWHM/2} \sin \theta d\theta = 2\pi \left[1 - \cos \left(\frac{FWHM}{2} \right) \right]$$

Equation 4.1

$$\Omega = 2\pi \left[1 - \cos \left(\frac{FWHM}{2} \right) \right]$$

Equation 4.2

The front-to-back ratio is simply the difference (since the units are in dB) between the peak transmission value and the transmission value in the back direction (180° behind the peak transmission value). The front-to-back ratio gives

a good estimate of how much radiation is creeping behind the cordless telephone and into the user's head. Hence, the front-to-back ratio tells a lot about surface wave suppression.

Define Ω_H as the horn's cross-section and Ω_A as the cross-section of the antenna on a high impedance electromagnetic surface. Then, the antenna efficiency η is the following:

$$\eta = \frac{\Omega_A}{\Omega_H} 10^{-\frac{\Delta}{10}},$$

Equation 4.3

where Δ is absolute value difference between the peak transmission values of the horn and antenna. The antenna efficiency above compares the efficiency of the antenna on a high impedance electromagnetic surface to the efficiency of the horn.

4.4. Experimental Results and Analysis

The previous section presented the method of analysis. Namely, it discussed the analysis of polar plots of the transmission radiation as a function of angular rotation. From the polar plots, the peak transmission value and FWHM can be obtained. From the FWHM, the cross-section can be computed. This is

done for two cases: one in which the transmission is between two identical horns, and another where the transmission is between only one of the horns and the antenna on a high impedance electromagnetic surface. The horn and antenna on a high impedance electromagnetic surface can then be compared to get the antenna efficiency.

The methodology discussed above has been done in the frequency range of 2.2 to 2.8 GHz. Since the band-gap is from 2.35 to 2.55 GHz, the frequency range analyzed has frequencies both inside and outside the band-gap.

The plot of the FWHM is Figure 4.5. In Figure 4.6, the cross-section is plotted. In Figure 4.7, the front-to-back ratio is plotted. In Figure 4.8, the antenna efficiency is plotted.

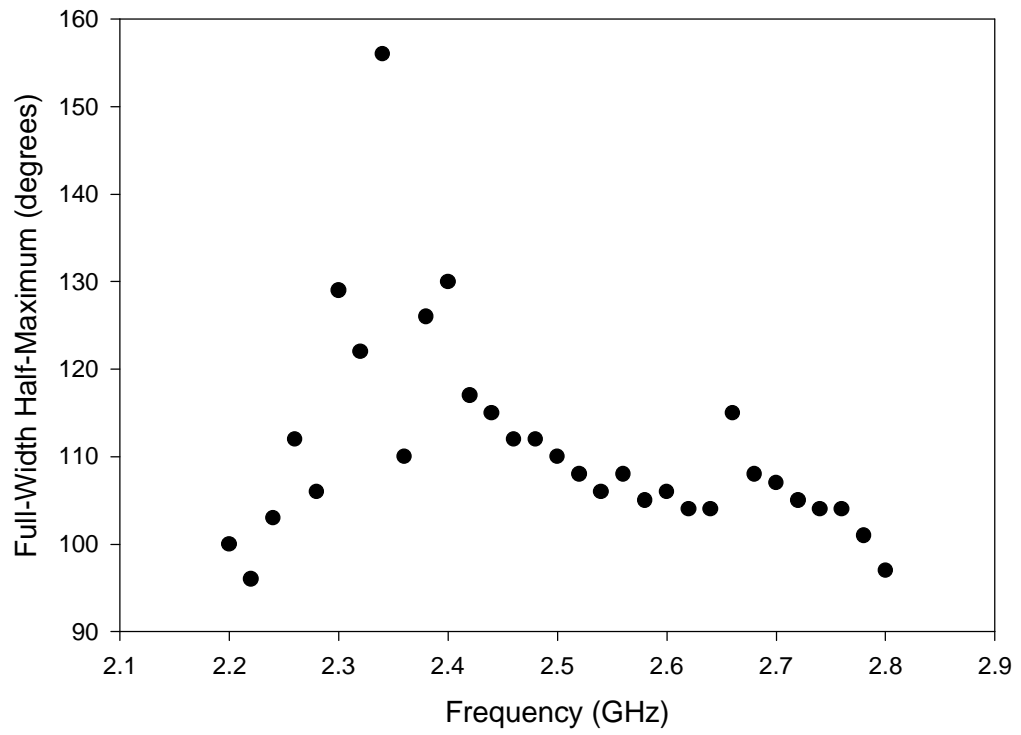


Figure 4.5: Plot of FWHM versus frequency.

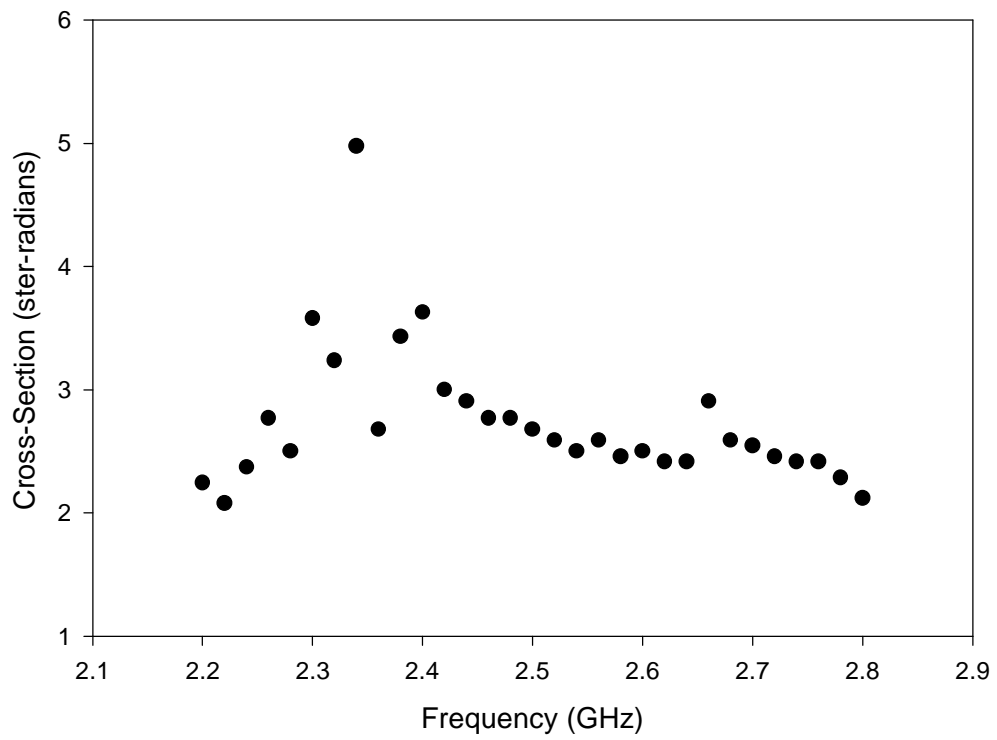


Figure 4.6: Plot of cross-section versus frequency.

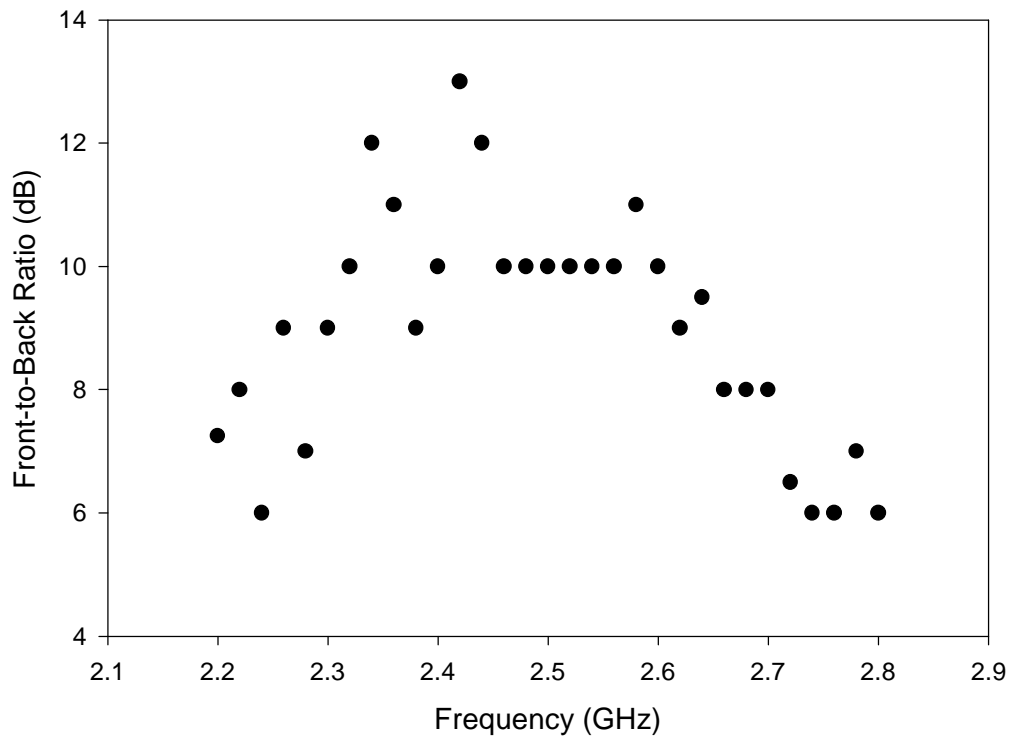


Figure 4.7: Plot of front-to-back ratio versus frequency.

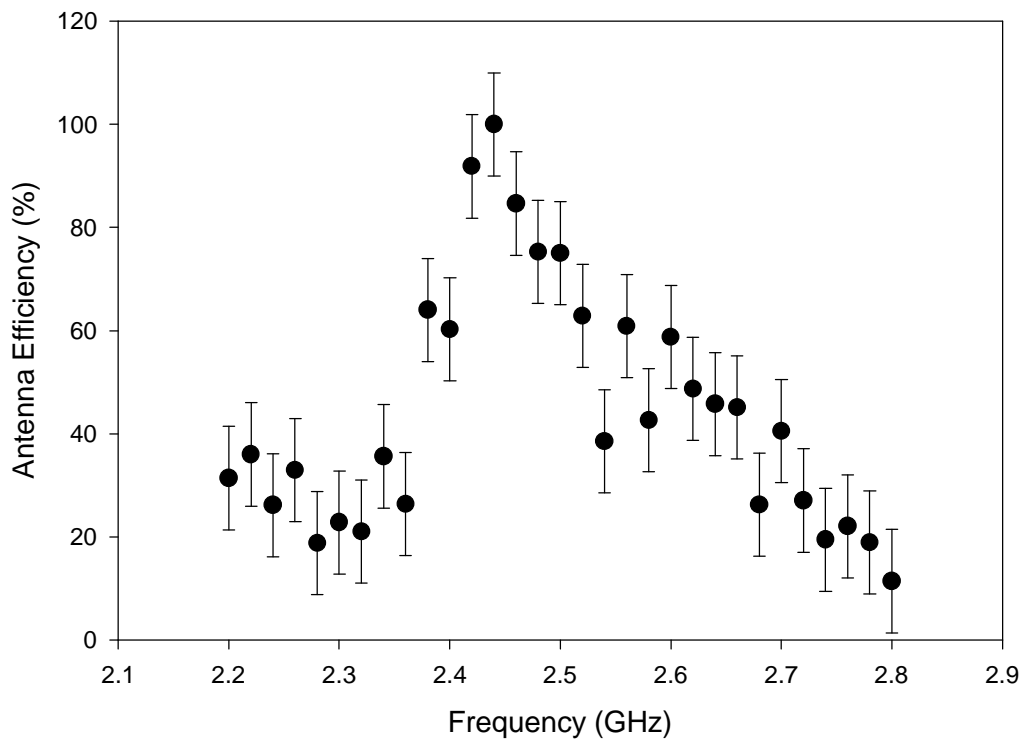


Figure 4.8: Plot of antenna efficiency versus frequency. The usable band is from 2.42 to 2.46 GHz, where the antenna efficiency is greater than 80%.

Several interesting observations can be made from Figures 4.5, 4.6, 4.7, and 4.8. From Figure 4.5, it can be seen that the FWHM in the band-gap tends to be low compared to the other frequencies. Since the cross section is derived from the FWHM, the cross-section plot of Figure 4.6 tends to show the same trend. Hence, it can be concluded that in the band-gap, half of the maximum transmitted powers are within smaller cross-sections than for frequencies outside the band-gap. In other words, the transmitted radiation in the band-gap is more directional and less broad than for frequencies outside the band-gap.

Figure 4.7 shows that within the band-gap, the front-to-back ratios are approximately 10 dB. Therefore, only about 10% of the emitted radiation are going behind the cordless telephone to be absorbed by the user's head. Compare this, however, to the performance of the frequencies outside the band-gap. The front-to-back ratios are about 7 dB for frequencies outside the band-gap. This translates to 20% of the emitted radiation going behind the cordless telephone to be absorbed by the user's head. Hence, for frequencies within the band-gap, the radiation going behind the cordless telephone is half compared to the radiation for frequencies outside the band-gap. This happens because in the band-gap frequency range, there is a suppression of surface waves.

Finally, in Figure 4.8, the antenna efficiency is plotted. It should be noted, however, that the plot is normalized to the peak antenna efficiency, which occurs at 2.44 GHz. It is no surprise that the peak antenna efficiency occurs at 2.44 GHz

because the center of the band-gap is theoretically designed for a frequency of 2.45 GHz.

It is interesting to note that before the normalization was done in the antenna efficiency, there is actually a frequency when the antenna on a high impedance electromagnetic surface has a higher efficiency than the horn. This frequency, of course, is where the peak antenna efficiency occurs, namely, 2.44 GHz. At 2.44 GHz, the unnormalized antenna efficiency η is equal to 1.017621, which means the antenna on a high impedance electromagnetic surface has antenna efficiency 1.76% greater than the horn. To normalize the antenna efficiency, 0.017621 was subtracted from all antenna efficiencies. This made the value of peak antenna efficiency to be 1.

Looking at the antenna efficiency plot, one can see that for frequencies near the center of the band-gap, the antenna efficiencies are quite high (above 80%). For frequencies not in the band-gap, however, the antenna efficiencies are very low (below 50%). Once again this phenomena can be explained by the properties of the high impedance electromagnetic surface. In the band-gap, there is a suppression of surface waves so that nearly all of the radiation is confined to one hemisphere. The peak gain of the antenna is higher and its radiation is more directional, and therefore the antenna efficiency is high. For frequencies not in the band-gap, there is no suppression of surface waves. A lot of the radiation leaks into the back of the antenna ground plane to be readily absorbed by the

user's head. The peak gain is lower, and the radiation not very directional.
Hence, the antenna efficiency is low.

Chapter 5: Application of High Impedance Electromagnetic Surfaces to Phased Arrays

5.1. Introduction

In the previous chapter, the high impedance electromagnetic surface suppressed surface waves, and consequently a user's head was effectively shielded from the antenna radiation. This antenna radiation shielding occurred in the photonic band-gap, which was from 2.35 to 2.55 GHz.

The suppression of surface waves by the high impedance electromagnetic surface can also be beneficial to phased arrays. If there are two or more antennas on the same high impedance electromagnetic surface (as in phased arrays), then the coupling between them will be reduced since surface wave propagation is a major contributor to inter-element coupling.

The result of using the high impedance electromagnetic surface as an antenna ground plane is the following: each antenna element in a multi-element antenna ground plane radiates as if it is isolated and is not surrounded by other neighboring antennas. The commercial implications of this conclusion are immense: antenna ground planes can be smaller, antenna ground planes can support more antenna elements, inter-element coupling is drastically reduced.

5.2. Experimental Setup

To study the suppression of surface waves by the high impedance electromagnetic surface, the basic setup shown in Figure 4.1 was used. However, the height of the rotating pedestal was lowered and the horn was tilted so that there is a fifteen degrees angle between the plane of the high impedance electromagnetic surface and the pointing direction of the horn. This setup is very similar to the Global Positioning System (GPS) configuration: the horn is like a user on earth, and the high impedance electromagnetic surface is the multi-element antenna ground plane of the GPS satellite system.

Schematically, the setup is shown below:

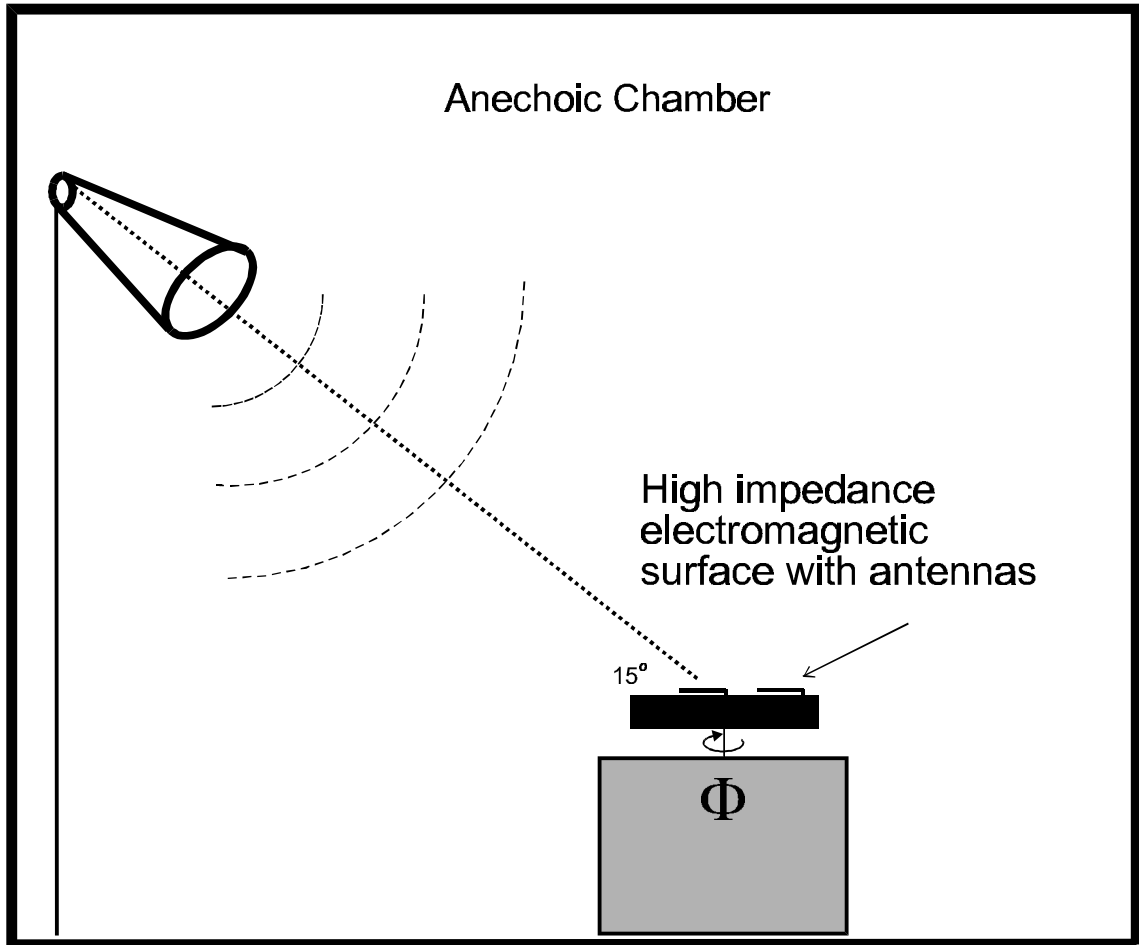


Figure 5.1: Experimental setup similar to the GPS configuration to study the suppression of surface waves by the high impedance electromagnetic surface.

The experimental protocol was very simple: first, a phase measurement was made with only one antenna present on the high impedance electromagnetic surface. This data was then stored on the memory (Memory 1) of the network analyzer. A second phase measurement was also taken, but two antennas are present on the high impedance electromagnetic surface instead of one. This data was also stored on the memory (Memory 2) of the network analyzer. Finally,

Memory 2 was subtracted from Memory 1 to see how the phase measurement was affected by the presence of the second antenna. This protocol was done for thirty degrees angle increments of the rotation angle Φ .

The second antenna was added in two ways to achieve two different layouts: the two antennas are in a straight line, and the two antennas are parallel to one another.

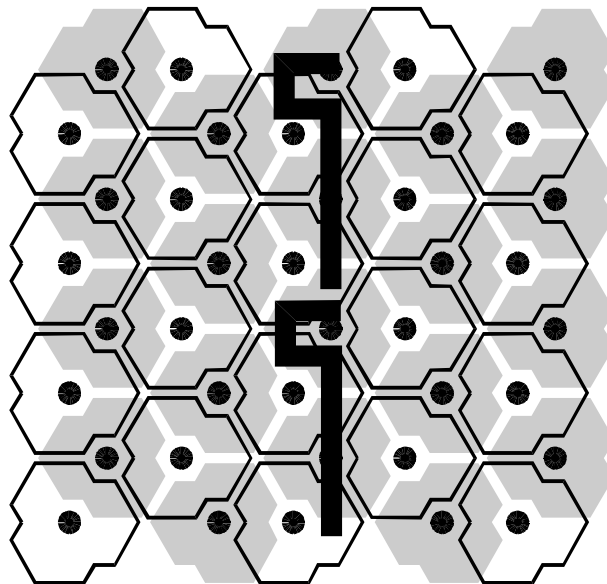


Figure 5.2: Two antennas are in a straight line.

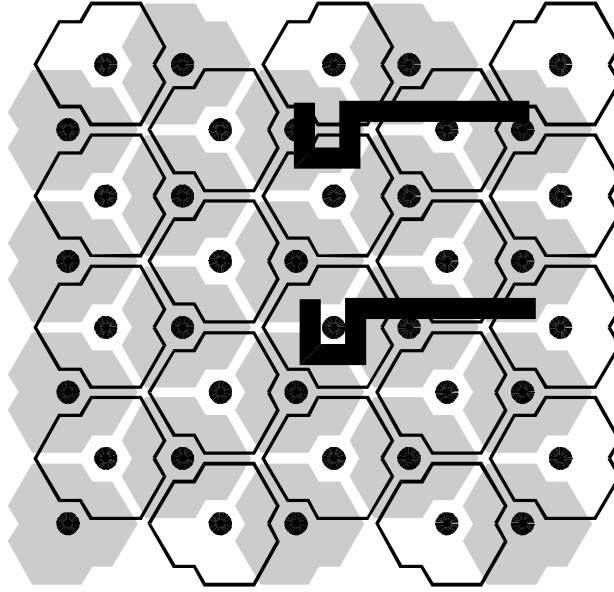


Figure 5.3: Two antennas are parallel to one another.

5.3. Experimental Results and Analysis

The polar plots shown in this section graph the phase difference as a function of the rotation angle. The polar angle is the rotation angle Φ , and as can be seen, the full rotation was done in increments of thirty degrees. The units of the rotation angle are in degrees. The radial variable is the phase difference due to the presence of the second antenna. Since phase was measured in degrees, the units of the phase difference are also in degrees.

Recall that the photonic band-gap is from 2.35 to 2.55 GHz. The three polar plots shown in Figure 5.4 are for three frequencies well within the photonic

band-gap: 2.4, 2.45, and 2.5 GHz. In this particular case, the two antennas are on a straight line as shown in Figure 5.2.

Now compare Figure 5.4 to Figure 5.5. In Figure 5.5, three polar plots are shown for frequencies not in the photonic band-gap: 2.2, 2.55, and 2.7 GHz. Like Figure 5.4, the two antennas are on a straight line.

Figures 5.4 and 5.5 are very different because one has frequencies in the band-gap and the other does not. For frequencies in the band-gap (Figure 5.4), there is very little phase difference variation for all rotation angles. To quantify this, the standard deviation from zero phase difference was calculated using the following formula, where the summation over i is done for all the rotation angles for one particular frequency:

$$\text{StandardDeviation} = \text{SD} = \sqrt{\frac{\sum_{i=1}^N \text{Phase Difference}_i^2}{N}}$$

Equation 5.1

The values of the standard deviation are shown in the legends of the respective figures. From Figure 5.4, the following values are obtained for frequencies in the band-gap: 2.4 GHz has SD=7.30 degrees, 2.45 GHz has SD=8.99 degrees, 2.5 GHz has SD=10.28 degrees. Likewise, from Figure 5.5, the following values are obtained for frequencies outside of the band-gap: 2.2 GHz has SD=35.95 degrees, 2.55 has SD=27.72 degrees, 2.7 has SD=18.83 degrees.

Quantitatively, it is clear that for frequencies outside of the band-gap, the deviation from zero phase difference is more pronounced than for frequencies in the band-gap. This is so because in the band-gap, there is a suppression of surface waves so that inter-element coupling between the two antennas is minimized. Outside of the band-gap, however, there is no suppression of surface waves and hence inter-element coupling is rampant.

Likewise, the same plots and conclusions can be done for the other layout, which is the case when the two antennas are parallel to one another. For frequencies in the band-gap (2.4, 2.45, and 2.5 GHz), the polar plots are shown in Figure 5.6. For frequencies outside the band-gap (2.2, 2.55, and 2.7 GHz), the polar plots are shown in Figure 5.7.

The phase difference for the parallel antennas layout (Figure 5.3) is greater than the phase difference for the straight antennas layout (Figure 5.2). This is observed to be true for all frequencies, both inside and outside of the band-gap. Intuitively, this makes sense, since in the parallel antennas layout, the two antennas are more likely to interfere than the straight antennas layout.

Nevertheless, the same trends can be observed in the parallel antennas layout as in the straight antennas layout. Namely, frequencies lying inside the band-gap have less phase difference than frequencies outside of the band-gap. The calculation of the standard deviations once again quantifies this phase difference as a function of frequency. In Figure 5.6, the following is obtained for frequencies in the band-gap: 2.4 GHz has $SD=23.28$ degrees, 2.45 GHz has

SD=26.17 degrees, and 2.5 GHz has SD=20.57 degrees. For comparison, in Figure 5.7, the following is obtained for frequencies outside of the band-gap: 2.2 GHz has SD=33.35 degrees, 2.55 GHz has SD=41.33 degrees, and 2.7 GHz has SD=61.44 degrees.

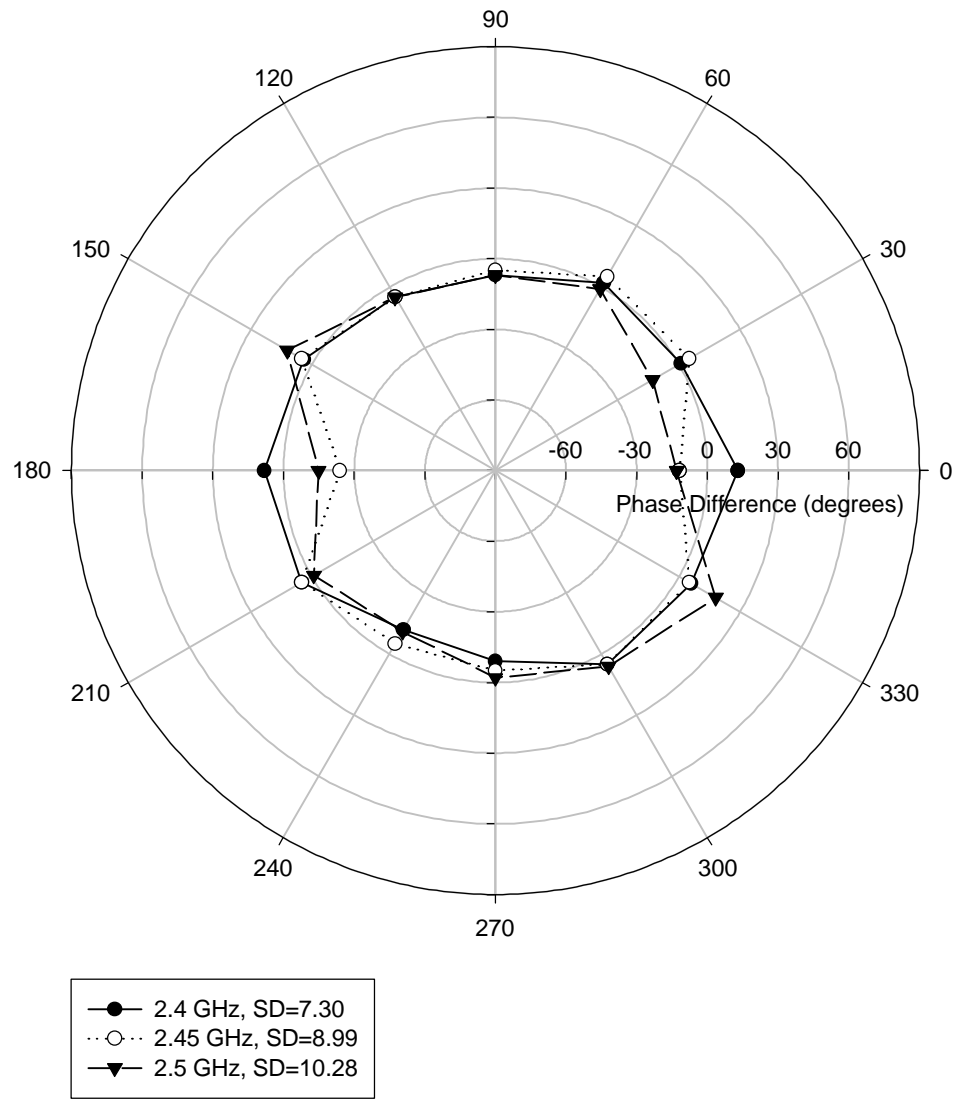


Figure 5.4: High impedance electromagnetic surface with antennas on a straight line. The frequencies plotted are inside the band-gap.

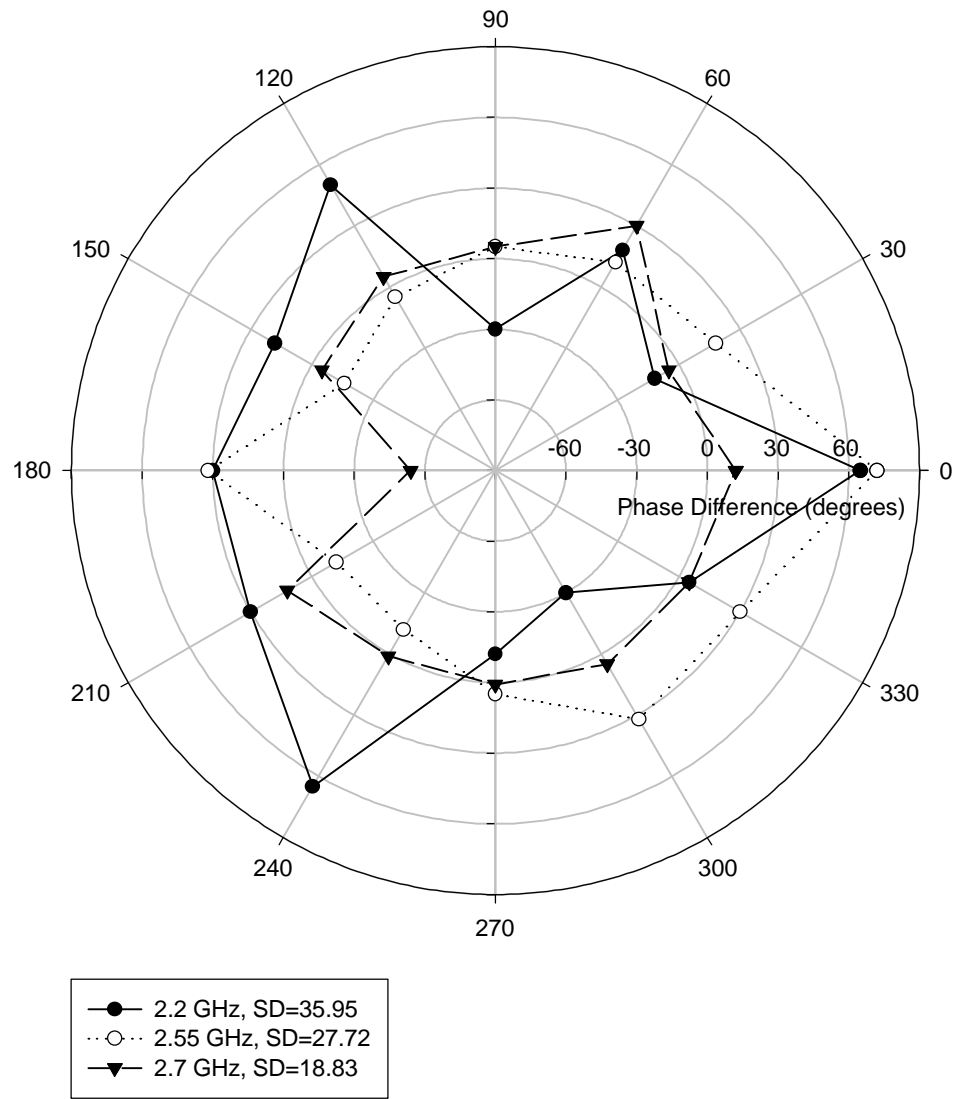


Figure 5.5: High impedance electromagnetic surface with antennas on a straight line. The frequencies plotted are outside the band-gap.

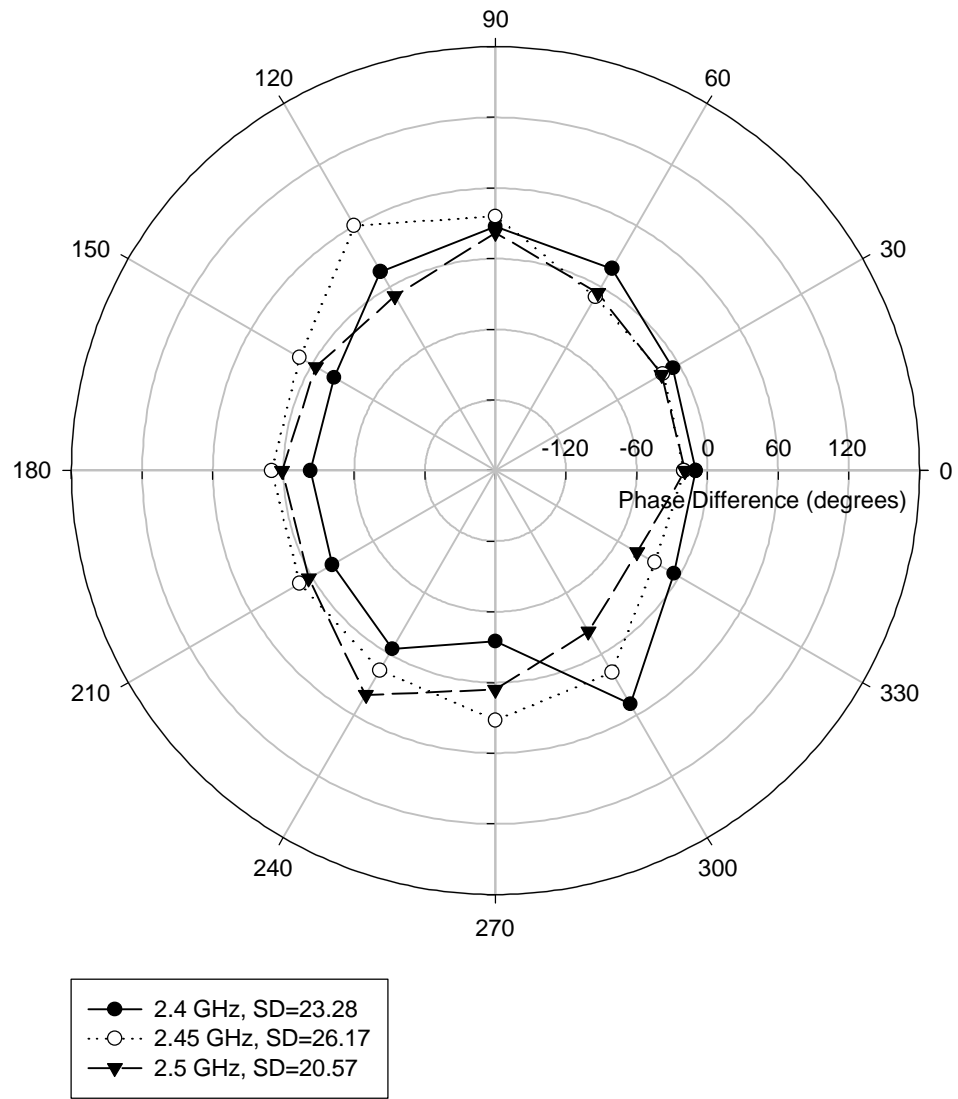


Figure 5.6: High impedance electromagnetic surface with antennas that are parallel to one another. The frequencies plotted are inside the band-gap.

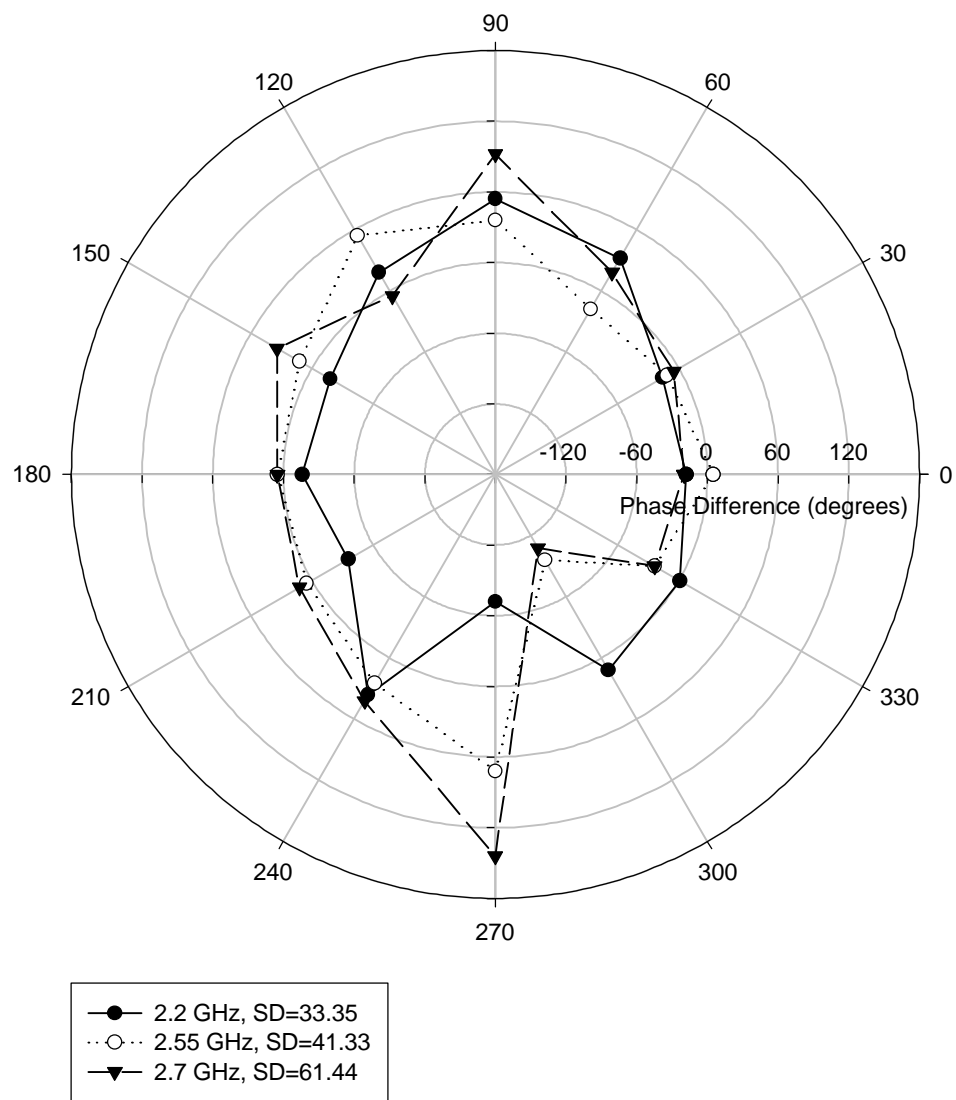


Figure 5.7: High impedance electromagnetic surface with antennas that are parallel to one another. The frequencies plotted are outside the band-gap.

5.4. Summary

The results are conveniently summarized in the table below. In the Frequency column, frequencies both inside and outside of the band-gap are listed in units of GHz. In the Straight column, the standard deviations are listed in degrees for the respective frequencies when the two antennas are in the straight layout. Similarly, in the Parallel column, the standard deviations are listed in degrees for the respective frequencies when the two antennas are in the parallel layout.

	Frequency	Straight	Parallel
Outside band-gap	2.20	35.95	33.35
	2.55	27.72	41.33
	2.70	18.83	61.44
Inside band-gap	2.40	7.30	23.28
	2.45	8.99	26.17
	2.50	10.28	20.57

Table 5.1: Summary of the standard deviations of the phase difference (in degrees) as a function of frequency (in GHz).

Looking at the standard deviations and polar plots from which they were calculated, a conclusion can be made concerning the use of high impedance electromagnetic surfaces as antenna ground planes for a multi-element phased array. Because of surface wave suppression, the phase difference due to inter-

element coupling is substantially less inside the band-gap as opposed to outside the band-gap.

Chapter 6: Conclusion

In this thesis, the high impedance electromagnetic structure was thoroughly investigated. In particular, the three-layer hexagonal structure was analyzed in the microwave frequency regime of 2.2 to 2.8 GHz. The band-gap of the three-layer hexagonal structure was designed to be from 2.35 to 2.55 GHz, and this band-gap was confirmed experimentally.

The high impedance electromagnetic surface was shown to be an effective antenna radiation shield. Acting as an antenna ground plane, it suppressed surface waves so that radiation is mainly confined to one hemisphere. Antenna gain is higher, and the radiation is more directional. Hence, the antenna efficiencies are high for frequencies inside the band-gap. For frequencies outside of the band-gap, however, the antenna efficiencies are low as radiation leaked behind the antenna ground plane.

Likewise, the ability of the high impedance electromagnetic surface to suppress surface waves was used in a phased array application. In the band-gap, there is a suppression of surface waves so that inter-element antenna coupling is minimized. Outside of the band-gap, the coupling between antenna elements is rampant so that one antenna greatly influences its neighboring antennas.

References

1. *High-Impedance Electromagnetic Surfaces*, by Daniel Frederic Sievenpiper.

University of California at Los Angeles dissertation, 1999.

2. *Mathematical Methods in the Physical Sciences, 2nd Edition*, by Mary L. Boas,

John Wiley & Sons, Inc., 1983.